Available online at www.sciencedirect.com
ScienceDirect
Nuclear Physics B Proceedings Supplement 00 (2014) 1–7
Nuclear Physics B Proceedings Supplement

Search for Higgs bosons decaying into photons at CMS

Matthew Kenzie on behalf of the CMS Collaboration

CERN, Route de Meyrin 385, 1217 Meyrin, Switzerland

Abstract

We present a new result in the search for Higgs bosons decaying into two photons at the CMS detector using the full LHC Run 1 dataset. The data samples correspond to integrated luminosities of 5.1 fb^{-1} and 19.7 fb^{-1} at centre-of-mass energies of 7 TeV and 8 TeV respectively. A clear signal is observed in the diphoton channel at a mass close to 125 GeV with a local significance of 5.7 σ, where 5.2 σ is expected from the standard model Higgs boson. The mass is measured to be 124.70 ± 0.34 GeV = 124.70 ± 0.31(stat) ± 0.15(syst) GeV and the signal strength relative to the standard model prediction is found to be $1.14^{+0.26}_{-0.23}$ = 1.14 ± 0.21(stat)$^{+0.09}_{-0.05}$(syst)$^{+0.13}_{-0.09}$(theo). Additional results include measurements of the signal strength modifiers with respect to different production mechanisms.

Keywords: Higgs, Standard Model, CMS, LHC, photon, symmetry

1. Introduction

In 2012, the ATLAS and CMS Collaborations announced the observation of a new particle whose properties where consistent with a SM Higgs boson with a mass around 125 GeV [1, 2]. The Higgs boson is the particle predicted to exist as a consequence of the spontaneous symmetry breaking mechanism in the electroweak section of the standard model (SM) [3, 4, 5, 6, 7, 8, 9]. Here we report on the search for the Higgs boson decaying into two photons at the CMS dectector. It summarises the work presented in Ref. [10] and is the first time this new result has been presented publicly. The diphoton decay channel provides a clean final state topology that allows the mass of the decaying object to be reconstructed with high precision. However there is a considerable amount of background originating from processes producing two prompt photons (about 70% of the selected events), one prompt photon and one neutral meson, where the meson is reconstructed as a photon (about 30% of the selected events), and two neutral mesons, where both are reconstructed as photons (less than 1% of selected events). Consequently the search consists of a small signal peak on a large falling background. Higgs bosons are produced in the LHC environment primarily through gluon fusion (ggH), about 88%, with smaller contributions from vector boson fusion (VBF), characterised by two forward jets, about 8%, and associated production with a W or Z (VH) or $t\bar{t}$ pairs (ttH), about 3% and 1% respectively. The decay of a Higgs boson into two photons primarily occurs via either a top loop or a W boson loop whose amplitudes destructively interfere resulting in a branching fraction of ∼0.2% for a SM Higgs at 125 GeV. Given the integrated luminsotity and centre-of-mass energies of the dataset used, around 5×10^5 SM Higgs bosons (with a mass of 125 GeV) can be expected to have been produced at CMS, of which about 1000 decay into two photons. The efficiency times acceptance of the analysis is about 50% for a signal with m_H = 125 GeV.

2. Analysis Strategy

The analysis is performed using the CMS experiment for which more details can be found in Ref. [11]. The diphoton invariant mass is reconstructed from the two photon four-vectors. This distribution is then fitted with background and signal components in order to extract properties of the signal. To improve the sensitivity,

by isolating events with similar resolution and signal to background ratios, the fit is performed simultaneously in several non-overlapping categories. The analysis strategy focuses on selecting two "good quality" photons (i.e. rejecting neutral mesons which fake photons in the detector), measuring their energy precisely and finding the primary vertex of the decay (hence determining the components of the photon four-vectors with good precision).

2.1. Photon energy

The photon energy is reconstructed by building clusters of energy deposits in the electromagnetic calorimeter. The algorithms used can be applied identically to electron showers and consequently the $Z \rightarrow e^+e-$ decay is used as a control channel for the analysis. A multivariate likelihood regression technique is used to correct individual photons' energies and provide an estimate of the per-photon energy resolution. The energy scale in data is then corrected as a function of data taking epochs, pseudorapidity (η), electromagnetic shower width (R_9[1]) and transerve energy (E_T), using the $Z \rightarrow e^+e^-$ channel. The photon energy resolution predicted by the Monte Carlo (MC) simulation is then made more realistic by adding a Gaussian smearing term derived as a function of data taking epochs, η and R_9 from the $Z \rightarrow e^+e_-$ channel.

2.2. Vertex location

Due to the running conditions of the LHC there can be several proton-proton collisions in each bunch crossing resulting in multiple primary vertices in each event. Consequently a boosted decision tree (BDT) is deployed to select the primary vertex from those of other interactions in the same bunch crossing. This uses information from the tracks which originate from each vertex and pointing from electron tracks in cases where one or more of the photons converts into an e^+e^- pair. An additional BDT is trained in order to assess the probability that the vertex choice was correct.

2.3. Photon Identification

A BDT is trained to reject photon candidates which originate in jets, mainly from π^0 mesons. Its inputs are variables which describe the electromagnetic shower shape and detector activity in a cone around the photon candidate (the hadronisation which produces neutral mesons typically results in non-isolated photon candidates). These variables are combined by the BDT to form a single output which provides an estimate of the per-photon quality. The distribution of this output is shown in Fig. 1 for mixed samples of prompt and fake photons. It can be seen that the data-MC agreement is very good and that the BDT effectively disinguishes between photon candidates which are real and fake.

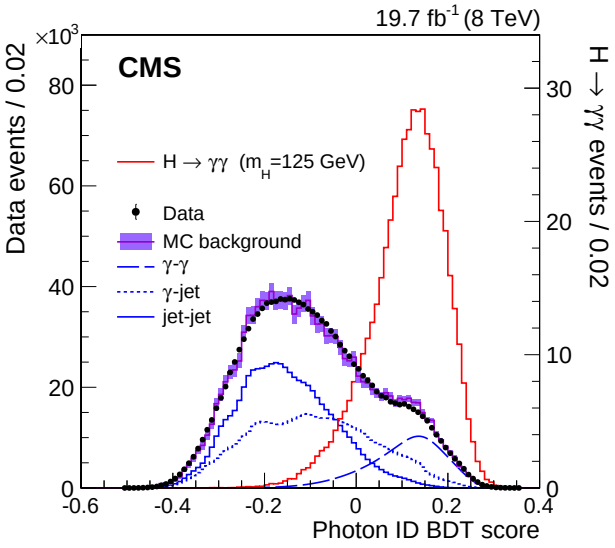

Figure 1: Photon identification BDT score of the lower-scoring photon of diphoton pairs. Shown for the 8 TeV dataset (points) and simulated background events (histogram with shaded bands) also broken down into events with either zero, one or two prompt photons. The tall solid histogram corresponds to simulated Higgs boson signal events.

3. Event classification

Events are separated into different event classes based on their topology, their mass resolution and their relative probability to be signal or background. The first step involves extraction of events tagged by the presence of additional objects in the final state (jets, leptons or missing transverse energy, E_T^{miss}) that give an event signature characteristic of particular production processes (VBF, VH or ttH). The remaining events are classified according to a variable constructed using multivariate techniques.

3.1. Multivariate event classifier

A multivariate event classifier, the diphoton BDT, is constructed in order to identify events which have good diphoton mass resolution and a high probability of being

[1]The R_9 is defined as the ratio of energy in the 3×3 array of crystals around the photon position to the energy of all the crystals in the supercluster (which can be anywhere between 25 and 175 crystals)

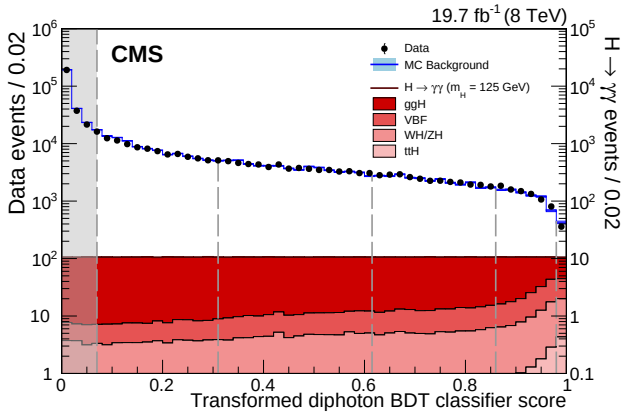

Figure 2: Transformed diphoton BDT classifier score for events in the 8 TeV dataset (points with error bars, left axis) and for simulated signal events from the four production processes (solid histograms, right axis). The outlined histogram following the data points is for simulated background events. The vertical dashed lines show the boundaries of the events classes, with the leftmost representing the score for below which events are discarded.

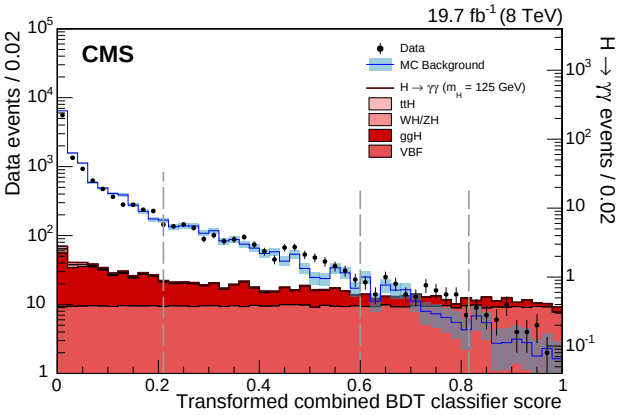

Figure 3: Transformed score of the combined dijet-diphoton BDT for events in the 8 TeV dataset (points with error bars, left axis) and for simulated signal events from the four production processes (solid histograms, right axis). The outlined histogram is for simulated background events. The vertical dashed lines show the boundaries of the dijet-tagged event classes with the leftmost representing the score for below which events are not included in the dijet-tagged classes but reclassified with the dihpton BDT.

signal rather than background. The classifier incorporates the ingredients detailed in Sec. 2: the photon identification BDT score of both photons, the probability the chosen vertex is correct, the energy resolution of both photons and other kinematic properties of the diphoton system. The output of the diphoton BDT, transformed to give a flat distribution for signal, is shown in Fig. 2 for signal, background and data events. It can be seen that a low score is assigned to background like events. The vertical dashed lines indicate the boundaries used to assign each event into a particular event class, which are optimised to give the smallest uncertainty on the signal yield. Events which fall below the lowest boundary (grayed region in Fig. 2) are cut out of the analysis.

3.2. *Events tagged by VBF-like production signatures*

Additional event classes are defined in order to isolate events which are likely to originate from a particular production process. VBF produced Higgs events result in two forward high transverse momenta jets. A BDT which includes jet variables is used to select events which are characteristic of this production mode. A further BDT is then used to couple the dijet BDT score with the diphoton BDT score (described in Sec. 3.1) in order to make use of all the additional information in the event. The output of this combined dijet-diphoton BDT score is then used to classify the selected events according to their probability to be produced by VBF. This distribution, transformed to be flat in VBF produced events, is shown in Fig. 3 for signal, background and data events. The vertical dashed lines indicate the boundaries used to assign each event to a particular class, which are optimised to give the smallest uncertainty on the VBF signal yield alone. Events which fall below the lowest boundary are not discarded but instead may be accepted as untagged events and classified according to the diphoton BDT described in Sec. 3.1.

3.3. *Events tagged by VH-like production signatures*

In these types of events Higgs bosons are produced in association with a W or Z boson resulting in additional leptons or E_T^{miss} in the final state. Four classes are defined: events with a muon or an electron are separated into two classes, according to whether there is significant E_T^{miss} or another lepton in the event, or there is not; a third class selects events with two or more jets; and the fourth class consists of events with large E_T^{miss}. Additional criteria are included to ensure that the charges of the tagged objects and their invariant mass are consistent with an additional W or Z boson. The selection criteria for these classes are optimised by minimising the expected uncertainty on the signal strength from these processes alone.

3.4. *Events tagged by ttH-like production signatures*

In these types of events Higgs bosons are produced in association with a t quark and a $\bar{t}$ quark resulting in b quarks and additional leptons or hadronic jets in the final state. The selection criteria require the presence of

at least one b-tagged jet and then either one additional jet and one electron or muon (leptonic $t\bar{t}$) or four additional jets and no lepton (hadronic $t\bar{t}$). The selection criteria for these classes is optimised by minimising the expected uncertainty on the signal strength from these processes alone.

3.5. Procedure of classification

In total there are 14 event classes for the 8 TeV dataset and 11 event classes for the 7 TeV dataset. To ensure the classes are mutually exclusive and the correct assignment of events is optimised, events are tested against the selection requirements of each class in a specific order: first the production-signature tagged classes ranked by expected signal-to-background ratio, then the untagged classes. Once selected, events are no longer candidates for inclusion in another class. The ordering, alongside the main selection requirements is shown in Table 1.

Table 1: Event classes for the 7 and 8 TeV datasets and some of their main selection requirements. Events are tested against the selection requirements of the classes in the order they are listed here.

Label	No. of classes 7TeV	8TeV	Main requirements
ttH lepton tag	⋆	1	$p_{\mathrm{T}}^{\gamma 1} > m_{\gamma\gamma}/2$ 1 b-tagged jet + 1 electron or muon
VH tight l tag	1	1	$p_{\mathrm{T}}^{\gamma 1} > 3m_{\gamma\gamma}/8$ [e or μ, $p_{\mathrm{T}} > 20$GeV, and $E_T^{\mathrm{miss}} > 45$GeV] or [$2e$ or 2μ, $p_{\mathrm{T}}^{l} > 10$GeV; $70 < m_{ll} < 110$GeV]
VH loose l tag	1	1	$p_{\mathrm{T}}^{\gamma 1} > 3m_{\gamma\gamma}/8$ e or μ, $p_{\mathrm{T}} > 20$GeV
VBF dijet tag 0-2	2	3	$p_{\mathrm{T}}^{\gamma 1} > m_{\gamma\gamma}/2$ 2 jets; classified using combined diphoton-dijet BDT
VH E_T^{miss} tag	1	1	$p_{\mathrm{T}}^{\gamma 1} > 3m_{\gamma\gamma}/8$ $E_T^{\mathrm{miss}} > 70$GeV
ttH multijet tag	⋆	1	$p_{\mathrm{T}}^{\gamma 1} > m_{\gamma\gamma}/2$ 1 b-tagged jet + 4 more jets
VH dijet tag	1	1	$p_{\mathrm{T}}^{\gamma 1} > m_{\gamma\gamma}/2$ jet pair, $p_{\mathrm{T}}^{\mathrm{j}} > 40$GeV and $60 < m_{\mathrm{jj}} < 120$GeV
Untagged 0-4	4	5	The remaining events, classified using diphoton BDT

⋆ For the 7TeV dataset, events in the ttH lepton tag and multijet tag classes are selected first, and combined to form a single event class.

4. Statistical modelling

4.1. Signal model

The signal shape is modelled using a sum of Gaussians (up to a maximum of 5) to describe the different resolution effects contributing to the diphoton invariant mass shape. The Gaussian parameters are obtained by fitting the shape to MC simulated events at different Higgs boson mass hypotheses and the parameter values are linearly interpolated in order to provide a description of the signal shape as a function of the hypothesis Higgs mass, m_H. This is done separately for each production process and in each analysis category where the signal efficiency is also obtained from MC simulation. The signal mass resolution varies considerably depending on the event class but in the best classes is as low as 1.05 GeV (for $m_H = 125$ GeV).

4.2. Background model

The background parametrisation is *a priori* unknown and given the considerable size of the background, a specific choice of its functional form can introduce large biases. A method, the discrete profiling method, has been developed [12] to treat the uncertainty associated with the choice of function used to fit the background in a similar way to systematic uncertainties associated with measurements. The choice of function used to fit the background is treated as a discrete nuisance parameter in the likelihood function used to extract the result. When performing a fit to the data, by minimising twice the negative likelihood, all reasonable function choices are considered and that which gives the minimum negative likelihood for a given configuration of the fit parameters is chosen. A penalty term is included into the likelihood to account for the number of free parameters in the fitting function, such that the penalised likelihood function, $\tilde{\mathcal{L}}_f$, for a given background fitting function, f, is defined as

$$-2\ln\tilde{\mathcal{L}}_f = -2\ln\mathcal{L}_f + N_f, \tag{1}$$

where $\mathcal{L}_f$ is the unpenalised likelihood and N_f is the number of free parameters in function f. It is found in tests made using pseduo-experiments that this value of the corrected likelihood gives consistently good coverage and neglible bias. These tests are performed for the individual analysis classes separately and for various combinations of them. Furthermore tests are performed for various different generating functions of the backgroundi distribution, and for cases when the generating function is not included as part of the discrete profiling choice. In all these cases the statistical properties of the method were found to be well behaved.

4.3. Systematic uncertainties

Several sources of systematic uncertainty are considered in the analysis. These are incorporated into the likelihood as nuisance parameters which affec the signal model. Whilst all the systematics considered contribute to the uncertainty on all measured properties, they can be grouped into two broad categories: those which predominantly affect the signal strength measurement (Table 2) and those which predominantly affect the mass measurement (Table 3).

4.3.1. Systematic uncertainties which contribute significantly to the signal rate measurement

The theoretical uncertainties on the signal yield are taken from the LHC Higgs Cross Section Working Group [13] and these make up the largest contribution to the signal yield uncertainty. The energy scale and resolution corrections applied to the data and MC have a corresponding uncertainty and this is propagated per-photon to the diphoton invariant mass distribution in each event class. Due to imperfect modelling of the shower shape variables and per-photon energy resolution estimate in the simulation an uncertainty is applied to account for events being misclassified by the diphoton BDT. There are various other smaller experimental effects such as luminosity uncertainty, trigger efficiency, vertex finding efficiency, selection efficiency, jet identification, lepton identification and E_T^{miss} measurement which are all accounted for and make small contributions.

4.3.2. Systematic uncertainties which contribute significantly to the mass measurement

The per photon scale and resolution correction uncertainties themselves contribute an uncertainty. Furthermore, because these corrections are derived from differences between data and MC simulation in $Z \to e^+e^-$ decays there are further effects which are considered. Firstly there is an uncertainty associated to the energy scale at which the corrections are derived. We assume a linear relation from m_z to m_H, this is checked with highly boosted Z bosons and a corresponding systematic uncertainty is added to account for any residual non-linearity. Secondly there are differences between electrons and photons in data which are not perfectly modelled in the simulation so there are further sources of systematic uncertainty which are added to account for this.

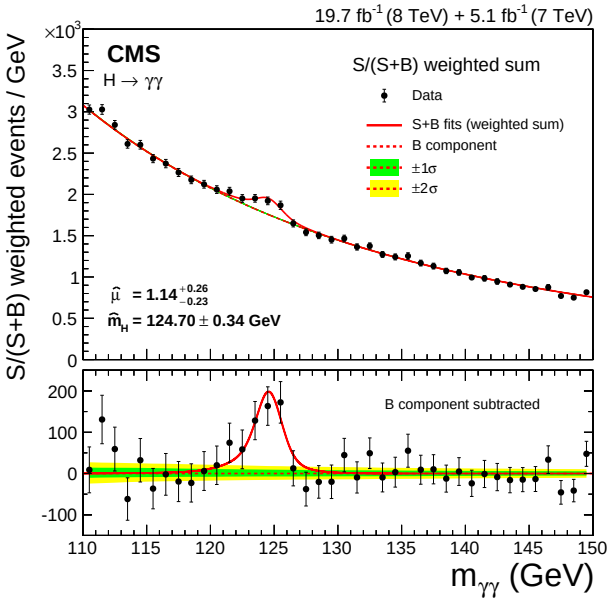

Figure 4: Diphoton invariant mass spectrum weighted by the ratio $S/(S+B)$ in each event class, together with the background substraced weighted mass-spectrum.

5. Results

The result of the simultaneous fit of the signal-plus-background when performed across all 25 analysis categories is shown in Fig. 4 where each of the events, as well as the fitted functions, are weighted by the ratio $S/(S+B)$ of the event category into which it falls.

5.1. Significance of the signal and its strength

The local p-value to observe a fluctuation of the background is shown as a function of the Higgs boson mass hypothesis, m_H, in Fig. 5. A significant excess is observed near 125 GeV with a local p-value of 5.7σ where 5.2σ is expected from the SM Higgs boson. The best fit signal strength as a function of m_H is shown in Fig. 6. The value of m_H corresponding to the maximum p-value is 124.7 GeV where the signal strength is observed to be $1.14^{+0.26}_{-0.23}$ relative to the SM prediction. The uncertainty contributions are shown in Table 2.

5.2. Mass measurement

To make the measurement of the mass of the observed resonance less model dependent the signal strengths of the production processes involving the Higgs coupling to fermions and the Higgs couplings to bosons are allowed to vary independently. These two signal strength modifiers are respectively denoted $\mu_{\text{ggH,ttH}}$ and $\mu_{\text{VBF,VH}}$ and defined relative to the SM prediction. Figure 7

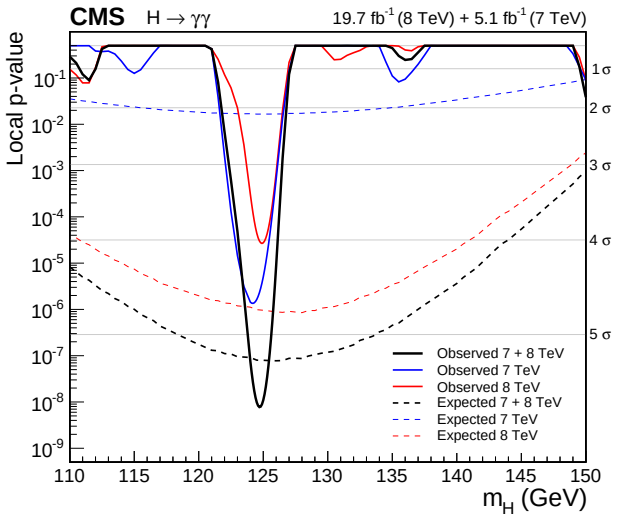

Figure 5: Local p-values as a function of m_H for the 7 TeV, 8 TeV and combined datasets. The expected values for a SM Higgs boson are shown as the dashed lines.

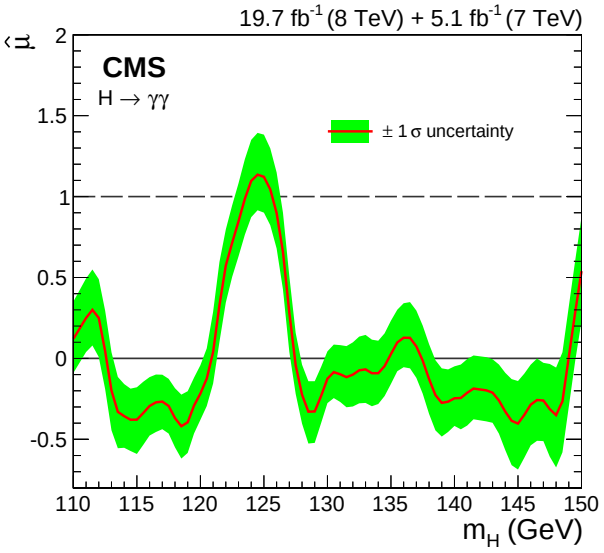

Figure 6: The best fit signal strength, relative to the SM prediction, as a function of m_H.

Source of uncertainty	**Uncertainty in $\hat{\mu}$**
Theoretical Predictions	0.11
Shower shape and resolution modelling	0.06
Energy scale and resolution	0.02
Other	0.04
All systematic uncertainties	0.13
Statistical	0.21
Total	**0.25**

Table 2: Magnitude of the uncertainty in the best fit signal strength, $\hat{\mu}$, induced by the systematic uncertainties in the signal model.

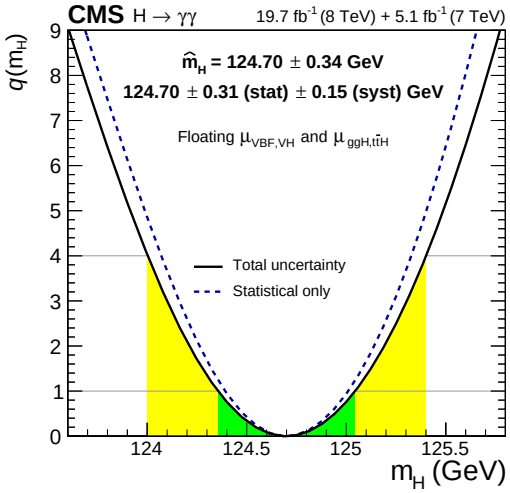

Figure 7: Scan of the likelihood ratio as a function of the hypothesis mass when $\mu_{\mathrm{ggH,ttH}}$ and $\mu_{\mathrm{VBF,VH}}$ are allowed to vary independently.

shows the resulting scan of the negative log likelihood ratio as a function of m_H. The best fit mass of the observed boson is found to be 124.70 ± 0.34 GeV. The uncertainty contributions are shown in Table 3.

5.3. Production mechanisms

The signal strength from individual production mechanisms is shown in Fig. 8 and the two dimensional scan of the likelihood ratio for the signal strength paramters to fermions and bosons, $\mu_{\mathrm{ggH,ttH}}$ and $\mu_{\mathrm{VBF,VH}}$, are shown in Fig. 9. It can be seen that the properties of the observed boson are consistent with the standard model prediction.

6. Summary

We report the observation of the diphoton decay mode of the recently discovered Higgs boson and the

Source of uncertainty	Uncertainty in $\widehat{m}_{\mathrm{H}}$ (GeV)
Imperfect simulation of e-γ differences	0.10
Linearity of the energy scale	0.10
Energy scale and resolution	0.05
Other	0.04
All systematic uncertainties	0.15
Statistical	0.31
Total	**0.35**

Table 3: Magnitude of the uncertainty in the best fit mass induced by the systematic uncertainties in the signal model.

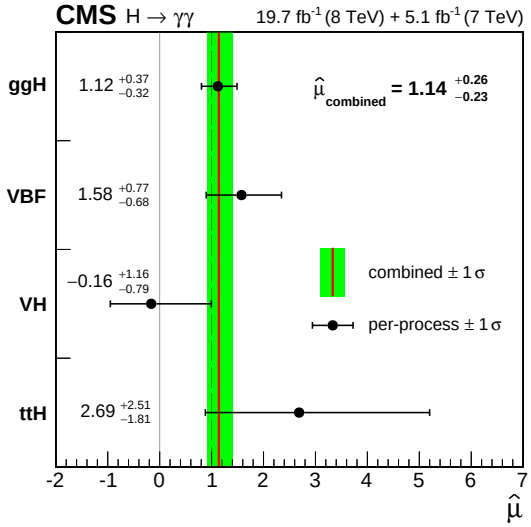

Figure 8: Best fit signal strength when the contribution from each of the production process is allowed to vary independently.

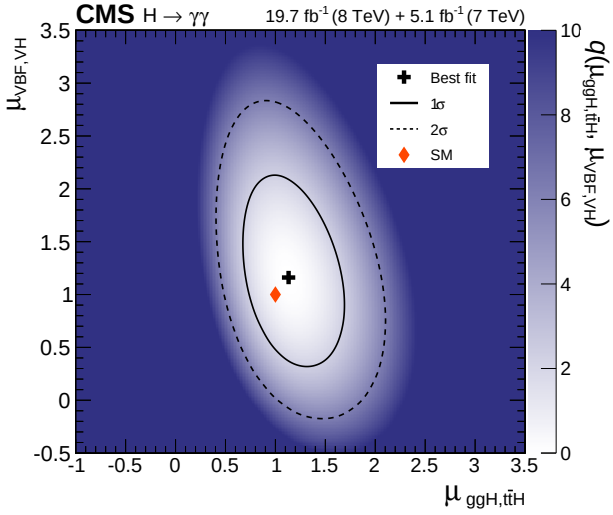

Figure 9: Scan of the likelihood ratio as a function of the signal strength from fermionic production processes, $\mu_{\mathrm{ggH,ttH}}$, versus bosonic production processes, $\mu_{\mathrm{VBF,VH}}$.

measurement of some of its properties. It is the first time this result and some of the new methodology of this analysis [10] have been publicly presented. The analysis uses the entire Run1 dataset collected by the CMS experiment during 2011 and 2012 LHC running. A clear signal is observed with a local significance of 5.7 σ when 5.2 σ is expected for a SM Higgs boson. The mass is measured to be 124.70 ± 0.34 GeV = 124.70 ± 0.31(stat) ± 0.15(syst) GeV and the signal strength relative to the standard model prediction is found to be $1.14^{+0.26}_{-0.23} = 1.14 \pm 0.21(\mathrm{stat})^{+0.09}_{-0.05}(\mathrm{syst})^{+0.13}_{-0.09}(\mathrm{theo})$. All the results are compatible with the expectations of a SM Higgs boson.

References

[1] The ATLAS Collaboration, Observation of a New Particle in the Search for the Standard Model Higgs Boson with the ATLAS Detector at the LHC, Phys. Lett. B 716 (2012) 1–29.

[2] The CMS Collaboration, Observation of a new boson at a mass of 125 GeV with the CMS experiment at the LHC, Phys. Lett. B 716 (2012) 30–61.

[3] P. W. Higgs, Broken symmetries, massless particles and gauge fields, Phys. Lett. 12 (1964) 132–133. doi:10.1016/0031-9163(64)91136-9.

[4] P. W. Higgs, Broken symmetries and the masses of gauge bosons, Phys. Rev. Lett. 13 (1964) 508–509. doi:10.1103/PhysRevLett.13.508.
URL `http://link.aps.org/doi/10.1103/PhysRevLett.13.508`

[5] F. Englert, R. Brout, Broken symmetry and the mass of gauge vector mesons, Phys. Rev. Lett. 13 (1964) 321–323. doi:10.1103/PhysRevLett.13.321.
URL `http://link.aps.org/doi/10.1103/PhysRevLett.13.321`

[6] G. S. Guralnik, C. R. Hagen, T. W. B. Kibble, Global conservation laws and massless particles, Phys. Rev. Lett. 13 (1964) 585–587. doi:10.1103/PhysRevLett.13.585.
URL `http://link.aps.org/doi/10.1103/PhysRevLett.13.585`

[7] S. L. Glashow, Partial-symmetries of weak interactions, Nucl. Phys. 22 (1961) 579. doi:10.1016/0029-5582(61)90469-2.

[8] S. Weinberg, A Model of Leptons, Phys. Rev. Lett. 19 (1967) 1264. doi:10.1103/PhysRevLett.19.1264.

[9] A. Salam, Weak and electromagnetic interactions, in: N. Svartholm (Ed.), Elementary particle physics: relativistic groups and analyticity, Almqvist & Wiskell, 1968, p. 367, proceedings of the eighth Nobel symposium.

[10] V. Khachatryan, et al., Observation of the diphoton decay of the Higgs boson and measurement of its propertiesarXiv:1407.0558.

[11] The CMS Collaboration, The CMS experiment at the CERN LHC, JINST 3 (2008) S08004. doi:10.1088/1748-0221/3/08/S08004.

[12] P. D. Dauncey, M. Kenzie, N. Wardle, G. J. Davies, Handling uncertainties in background shapes: the discrete profiling method, *To be submitted to* JINST (2014). arXiv:1408.6865.

[13] LHC Higgs Cross Section Working Group, Handbook of LHC Higgs cross sections: 3. Higgs Properties, CERN Report CERN-2013-004 (2013). arXiv:1307.1347, doi:10.5170/CERN-2013-004.

[14] H. Akaike, A new look at the statistical model identification, IEEE Transactions on Automatic Control 19 (1974) 716. doi:10.1109/TAC.1974.1100705.